

Under-ice acoustic navigation using real-time model-aided range estimation

EeShan C. Bhatt,^{1, 2, a} Oscar Viquez,² and Henrik Schmidt²

¹*MIT-WHOI Joint Program in Oceanography/Applied Ocean Science & Engineering,
Cambridge and Woods Hole, MA, USA*

²*Department of Mechanical Engineering, Massachusetts Institute of Technology,
Cambridge, MA*

(Dated: 20 February 2022)

1 The long baseline (LBL) underwater navigation paradigm relies on the conversion
2 of recorded travel times into pseudoranges to trilaterate position. For real-time op-
3 erations, this conversion has assumed an isovelocity sound speed. For re-navigation
4 in post-processing, computationally and/or labor intensive acoustic modeling may
5 be employed to reduce uncertainty driven by multipath arrivals. This work demon-
6 strates a real-time ray-based prediction method of the effective sound speed along
7 a path from source to receiver to minimize vehicle position error. This method was
8 implemented for a small scale AUV-LBL system in March 2020, in the Beaufort Sea,
9 in total ice-covered conditions and a double ducted acoustic propagation environ-
10 ment. The vehicle was successfully deployed and recovered. Given the lack of GPS
11 data throughout the vehicle’s mission, however, the pseudorange performance is first
12 evaluated on connections between GPS-linked beacons. The real-time ranging error
13 between beacons is roughly 11 meters at distances up to 3 km. But a consistent over-
14 estimation in the real-time method provides insights for improved eigenray filtering
15 by the number of surface bounces. An operationally equivalent pipeline is used to
16 re-position the LBL beacons and re-navigate the AUV, using a modeled, historical,
17 and a locally observed sound speed profile. The median re-navigation error is 1.84 ± 2.19 RMS m. The improved trilateration performance for suggests that this ap-
18 proach effectively extends the single meter accuracy of the deployed GNSS units into
19 the water column.

^aebhatt@whoi.edu

²¹ **I. INTRODUCTION**

²² Autonomous underwater vehicles (AUVs) are increasingly capable platforms to explore
²³ and sample the ocean, particularly for remote and/or dangerous regions. However, navi-
²⁴ gation uncertainty is a major challenge in considering AUVs as standard tools for oceano-
²⁵ graphic research. While land and air-based robots utilize information from Global Naviga-
²⁶ tion Satellite Systems (GNSS) to achieve stunning location accuracy and precision through-
²⁷ out the duration of their missions, AUVs cannot access GNSS fixes while underwater. There-
²⁸ fore, underwater vehicles have relied on any combination of dead reckoning, hydrodynamic
²⁹ models, inertial navigation systems, doppler velocity logs, and acoustic baseline positioning
³⁰ systems for navigation (Paull *et al.*, 2014). Limiting navigation error and drift requires an
³¹ AUV to periodically stall on the surface and obtain a GNSS fix to reset its position error.
³² This foolproof method of self-positioning is undesirable for stealth, adverse weather condi-
³³ tions, and mission efficiency, and inaccessible in a GNSS-denied situation like an ice-covered
³⁴ environment.

³⁵ Of underwater acoustic navigation systems, long baseline (LBL) is the most GPS-like
³⁶ in style and scale, and most appropriate for mitigating drift without overburdening com-
³⁷ putation or payload size on the vehicle (Van Uffelen, 2021). The state-of-the-art for LBL
³⁸ outsources depth to a pressure sensor and solves the two-dimensional localization problem
³⁹ with an isovelocity, linear scaling between one way travel time (OWTT) and range (Eustice
⁴⁰ *et al.*, 2006, 2007; Webster *et al.*, 2009, 2012). This assumption is valid for short scale
⁴¹ operations but oversimplifies propagation for larger and/or complex acoustic environments.

42 To achieve single meter, GNSS-like performance in a GNSS-denied environment, we demon-
 43 strate an embedded ray-based data processing algorithm to convert recorded OWTTs into
 44 pseudorange estimates. This methodology was integrated onto the AUV *Macrura*, deployed
 45 and recovered in the Beaufort Sea, in March 2020, during the Ice Exercise 2020 (ICEX20).
 46 A physics-driven methodology that received an *in situ* sound speed profile (SSP) was nec-
 47 essary despite the small operational domain because of the relatively high-risk mission en-
 48 vironment—total under-ice conditions and a variable double ducted acoustic environment.
 49 For consistency, we delineate specific definitions for timing, positioning, and navigation
 50 from [Howe et al. \(2019\)](#).

- 51 1. Timing is the ability to acquire and maintain accurate and precise time anywhere in
 52 the domain of interest within user-defined timeliness parameters
- 53 2. Positioning is the ability to accurately and precisely determine one's location refer-
 54 enced to a standard geodetic system
- 55 3. Navigation is the ability to determine current and desired position (relative or absolute)
 56 and apply corrections to course, orientation, and speed to attain a desired position
 57 anywhere in the domain of concern

58 Thus, navigation is inherently in real-time and depends on positioning; positioning depends
 59 on timing. We also suggest re-navigation and re-positioning as post-processed corollaries,
 60 which may include knowledge or processing capabilities not available *in situ*.

61 While RAFOS floats championed one way ranging for re-positioning ([Duda et al., 2006](#);
 62 [Rossby et al., 1986](#)), the ability to do so for navigation was facilitated by the advent of

the WHOI Micro-Modem (Singh *et al.*, 2006) and synchronized clocks (Rypkema *et al.*, 2017). AUV navigation efforts have achieved root mean square (RMS) localization error on the order of tens of meters relative to GNSS surface position over less than ten kilometers in shallow (Claus *et al.*, 2018; Eustice *et al.*, 2007; Kepper *et al.*, 2017) and deep water (Jakuba *et al.*, 2008; Kunz *et al.*, 2008; Webster *et al.*, 2009). However, these efforts all used a nominal sound speed for travel time conversion and the vehicles were limited to shallower isovelocity regimes.

Localization algorithms that do consider environmental or acoustic uncertainty tend to focus on longer and larger experiments, where spatio-temporal variability cannot be ignored. These methods have also been reserved for post-processing as they can be labor intensive, computationally heavy, and/or require additional information like contemporaneous data. For example, gliders navigating with kinematic flight models and equipped with acoustic modems were later unambiguously associated with predicted ray arrivals, resulting in roughly a kilometer error and hundred meters uncertainty over basin scale propagation (Van Uffelen *et al.*, 2013). A follow up study investigated how a single temporally and spatially averaged SSP could mitigate position error for a four month glider mission (Uffelen *et al.*, 2016). Wu *et al.* (2019) cross correlate three days of real acoustic records with synthetic ones generated through ocean model snapshots from HYCOM (Chassagnet *et al.*, 2007). While potentially applicable for various ocean states, this is reliant on model realism and impractical for real-time operations. Mikhalevsky *et al.* (2020) introduces a “cold start” algorithm that does not require prior knowledge of track, position, or sound speed information. The algorithm inputs a four-dimensional ocean model, constrained by tomography data, into a range dependent

85 ray code to isolate the last path detected in a full multipath pattern. Then, a representative
86 group speed is solved for alongside position in a least squares fashion. This approach is able
87 to re-position a floating hydrophone array with an error of 58 m and a standard deviation
88 of 32 m based on six sources 129–450 km away but remains to seen for real-time navigation.

89 The ICEX20 AUV deployment necessitated an environmentally- and physically-driven
90 relationship between recorded travel times and estimated pseudoranges due to the multipath
91 uncertainty brought upon by an increasingly observed double ducted environment in the
92 Beaufort Sea, which some refer to as the “Beaufort Lens” (Chen *et al.*, 2019; Chen and
93 Schmidt, 2020; Litvak, 2015).

94 Given that a lens introduces significant ray refraction, the Beaufort Lens is a shorthand for
95 the spatio-temporal variability of the local temperature and sound speed maxima generally
96 around 50 to 60 m in depth. A neutrally buoyant layer of warm Pacific Summer Water
97 creates a unique double ducted environment —the upper duct degrades signal coherence
98 due to intensified ice interaction and the lower duct effectively traps sound for long range
99 propagation (Poulsen and Schmidt, 2017). Modeling output (Duda *et al.*, 2021, 2019) and
100 experimental observations (Ballard *et al.*, 2020; Bhatt, 2021) suggest that, in the Beaufort
101 Sea, the duct is persistent and widespread but not necessarily continuous; it and its acoustic
102 effects can be non-existent, minimal, or drastic. Transmissions in the upper duct, between
103 the surface ice and the lens, experience minimal attenuation but degrade in signal coherence
104 with repeated reflections under the ice. In lower duct, between the lens and its conjugate
105 depth in the Atlantic water, roughly 200 m, sound above 350 Hz is trapped near losslessly
106 for long range propagation (Poulsen and Schmidt, 2017).

107 Thorough reviews of uncrewed vehicle operations in polar environments can be found in
108 (Norgren *et al.*, 2014) and (Barker *et al.*, 2020); there is no comparable work in the Arctic
109 for a short range AUV deployment in the Beaufort Lens. Seminal (Bellingham *et al.*, 1995;
110 Brooke, 1981; Hayes and Morison, 2002; Jackson, 1983; Light and Morison, 1989) and more
111 recent AUV deployments (Fossum *et al.*, 2021; Jakuba *et al.*, 2008; Kukulya *et al.*, 2010;
112 Kunz *et al.*, 2008; Plueddemann *et al.*, 2012; Timmermans and Winsor, 2013) witnessed the
113 classical upward refracting sound speed profile that is amenable to an isovelocity assumption.

114 Of note, despite different platforms and scales, are recent glider deployments in the
115 Canada Basin. In 2014, in partially ice-covered conditions, a long range LBL system with
116 WHOI Micro-Modems at 100 m exploited the lower duct for long range communication with
117 two gliders (Freitag *et al.*, 2016; Webster *et al.*, 2015). The sound speed value measured at
118 the time of reception was used to estimate pseudorange in post-processing. The beacon-to-
119 beacon performance was excellent, achieving contact at ranges greater than 200 km with
120 a position uncertainty of 40 m. The beacon-to-glider performance, however, deteriorated
121 due to missed contacts outside the duct, and was not described quantitatively. In 2017,
122 gliders were deployed in a region with no ice coverage (Graupe *et al.*, 2019). Ranges were
123 linearly scaled by a statistical description of sound speed observations taken during the
124 experiment, 1450 ± 6.5 m/s. This resulted in an error of 550 m, which was reduced by
125 a factor between 4 and 5, depending on the dive, using a post-processing acoustic arrival
126 matching method. Both cases exploit the lower duct for high fidelity communication at
127 long ranges. Unintuitively, the smaller nature of our deployment during ICEX20 is not a

¹²⁸ simplifying factor. For source depths typical to vehicle operations, 30 to 200 m, a shadow
¹²⁹ zone spans from 2 to 6 kilometers in range ([Schmidt and Schneider, 2016](#)).

¹³⁰ Compared to the previous small scale navigation efforts, the approach in this paper
¹³¹ integrates real-time model-aided data processing to estimate a representative sound speed
¹³² along a path from source to receiver, leveraging climatology, *in situ* data, and fast acoustic
¹³³ modeling. The paper is organized as follows. Section [II](#) details the experimental approach
¹³⁴ and conditions during ICEX20. Given that there is no GNSS ground truth for the vehicle
¹³⁵ position while underway, we first evaluate the real-time ranging performance of GPS-linked
¹³⁶ beacon-to-beacon communication events in section [III](#). Section [IV](#) uses insights from field
¹³⁷ data to introduce a new ray filtering algorithm to improve range estimation. Section [V](#)
¹³⁸ emulates the real-time processing pipeline to re-position beacon-to-beacon events and re-
¹³⁹ navigate AUV *Macrura*.

¹⁴⁰ **II. OVERVIEW OF THE ICEX20 EXPERIMENT**

¹⁴¹ The results from this paper derive from data taken while deploying the AUV *Macrura*, a
¹⁴² custom Bluefin-21, during the Ice Exercise 2020 (ICEX20), in the Beaufort Sea, from March
¹⁴³ 8th to 11th. The AUV deployment was supported by the Integrated Communication and
¹⁴⁴ Navigation Network (ICNN) ([Randeni et al., 2020, 2021; Schneider et al., 2020](#)), a special-
¹⁴⁵ ized implementation of the LBL solution. The ICNN was initially developed via numerous
¹⁴⁶ virtual experiments to ensure robust algorithms and interfaces between different hardware
¹⁴⁷ components. The simulation capabilities are largely physics-driven with a modular system of
¹⁴⁸ systems approach—an environmental simulator with sub-components for the ocean, includ-
¹⁴⁹ ing Arctic ice drift and ocean acoustic propagation; a vehicle simulator with sub-components
¹⁵⁰ for vehicle dynamics and navigation; a topside hardware simulator and acoustic communica-
¹⁵¹ tions simulator, both with a software-only configuration and a hardware-in-the-loop version
¹⁵² ([Schneider and Schmidt, 2018](#)). The virtual environment similarly emulates the interfaces
¹⁵³ between the real components to test the entire software pipeline.

¹⁵⁴ **A. The Integrated Communication and Navigation Network**

¹⁵⁵ The ICNN is comprised of four ice buoys in a loose rectangle, roughly 2 km away from
¹⁵⁶ a central ice camp with a topside computer, as shown in Fig. 1. The AUV and each ice
¹⁵⁷ buoy are outfitted with a WHOI Micro-Modem ([Singh et al., 2006](#)), with a four-element
¹⁵⁸ receiver array, a single transmitter, and one-tenth of a millisecond resolution. Acoustic
¹⁵⁹ messages were sent with a 10 kHz carrier frequency, 5 kHz bandwidth, and phase-shift

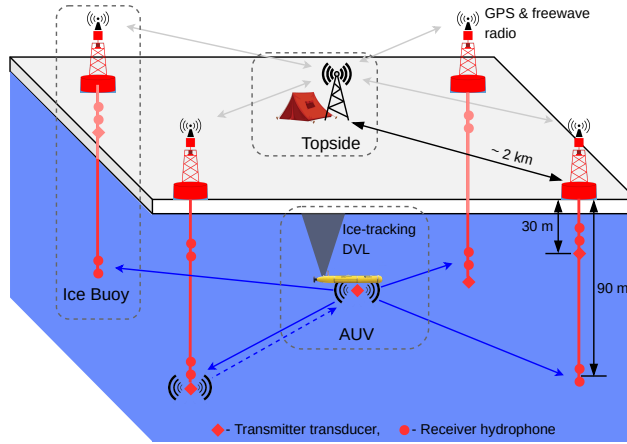


FIG. 1. A schematic overview of the Integrated Communication and Navigation Network (ICNN), which provides joint data-transfer and tracking between AUV and a human decision maker at Topside.

keying (PSK)modulation on a time-division multiple access schedule with a thirty-second cycle, giving room for two-way communication throughout the mission volume. The receive and transmit elements were split between shallow and deeper depths—30 and 90 m—to provide better coverage across the shadow zone. While each buoy only has one transmit depth, all buoys have both receive depths but the active receive layer is consistent across all buoys. The design of the ICNN enables a self-adapting network to transmit and receive at the optimal depth to maintain contact with the AUV ([Schneider *et al.*, 2020](#)). The buoys do not encompass the full horizontal range of the vehicle but are positioned to minimize overlap in trilateration for spherical positioning ([Deffenbaugh *et al.*, 1996a](#)).

To balance competing uses of the acoustic channel, the network uses a single synchronized digital communication packet to provide both tracking and data to the operator.

171 1. The AUV, running an ice-tracking DVL and an onboard hydrodynamic model, broad-
172 casts its perceived location on a scheduled, time-synchronized message via WHOI
173 Micro-Modem

174 2. Four ice buoys, each outfitted with a WHOI Micro-Modem, receive messages from the
175 AUV and send that information over freewave radio to a Topside computer

176 3. The topside computer converts travel times into pseudorange estimates using a stochas-
177 tic embedded prediction of the horizontal group velocity via BELLHOP ray tracing
178 code ([Porter, 2011](#)) using a sound speed profile provided by an updatable Virtual
179 Ocean ([Bhatt *et al.*, 2022; Schneider and Schmidt, 2018](#))

180 4. The topside computer calculates a new position by trilaterating the range estimates

181 5. The position differential, not the absolute position, is broadcast to the vehicle to
182 update its navigation solution and be robust to latency and intermittency

183 In the face of GNSS-denied navigation, this approach was anecdotally successful, as shown

184 in Fig. 2. The AUV *Macrura* was deployed through a hydrohole from an ice camp but re-

185 covered through an emergency hydrohole. A random disk error stalled *Macrura* underneath

186 the ice but did not prevent it from transmitting its location. Due to an incoming storm, a

187 team placed a physical marker on the ice at the location. Three days later, *Macrura* was

188 found within a meter of the marker. We view the emergency recovery as qualitative proof

189 of the robustness of this navigation approach. Nonetheless, this paper specifically addresses

190 the third and fourth steps—the conversion of travel times into pseudoranges and its effect

191 on trilateration. By focusing on pseudorange estimates between GPS-tracked beacons, and

re-running the trilateration pipeline, the results are decoupled from all other mechanisms in the ICNN.

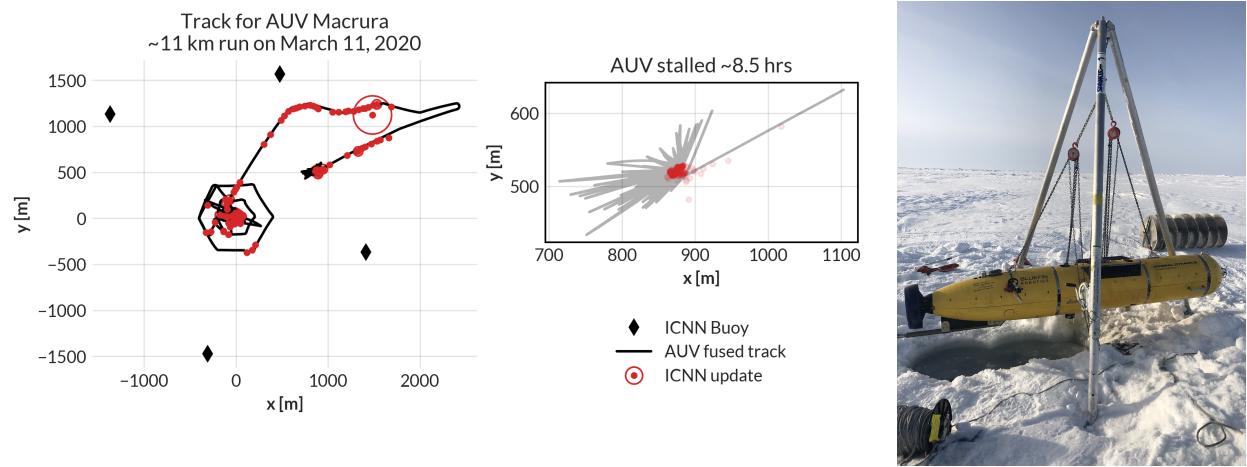


FIG. 2. The under-ice mission track for AUV *Macrura*, including the position updates as it stalled underneath the ice overnight. A marker was placed on the ice at the vehicle's estimated self-location. It was recovered after a three day storm within a meter of the marker.

194 B. ICEX20 sound speed conditions

An important component to our navigation solution is an accurate estimation of a representative SSP for the ocean volume. Previous field experience, during the Ice Exercise 2016 (ICEX16), demonstrated the negative effects of the Beaufort Lens on tracking and communication (Schmidt and Schneider, 2016). Fig. 3 shows historical, modeled, and *in situ* sound speed data for both ICEX16 and ICEX20. These three input streams were selected to mirror the information available on a submarine (personal conversation with LT B. Howard and LT CDR D. Goodwin). In the field, the SSP information was shared with the vehicle via basis

representation compression on a lightweight digital acoustic message (Bhatt *et al.*, 2022). All modeled data comes from HYCOM (Chassignet *et al.*, 2007), which does not seem to capture the forcing mechanisms that cause the Beaufort Lens. For ICEX16, the data-driven profile was sourced from nearby Ice Tethered Profilers (ITP) after the field experiment (Krishfield *et al.*, 2008; Toole *et al.*, 2011) and exhibits a fairly low lens; the historical profile is from the World Ocean Atlas. For ICEX20, the chosen weights (data-driven) profile derives from an estimate of initial CTD casts taken on site, showing an intense warm water intrusion; the baseline (historical) profile, showing moderate ducted conditions, comes from the average of March 2013 ITP data. This month best matched sea ice and sound speed conditions at the beginning of ICEX20 (Bhatt *et al.*, 2022). It is important to note that all profiles that do show the Beaufort Lens do so with different local sound speed maxima at different depths, reflective of the wide range of lens properties observed for all ITP data in the region. The variability of the lens height and prominence is the main reason an updatable SSP was integrated into the ICNN solution.

During ICEX20, the HYCOM profile was available but never deployed. For post-processing comparison, we introduce both the HYCOM profile and an isovelocity case, 1441.8 ± 3.7 m/s, as the mean and standard deviation of the observed sound speed profile over the first 200 m. This is a contrived value taken in the style of Graupe *et al.* (2019) for the sake of comparison; the default value in the LAMSS simulator, which was not environmentally informed nor used during ICEX20, was 1430 m/s.

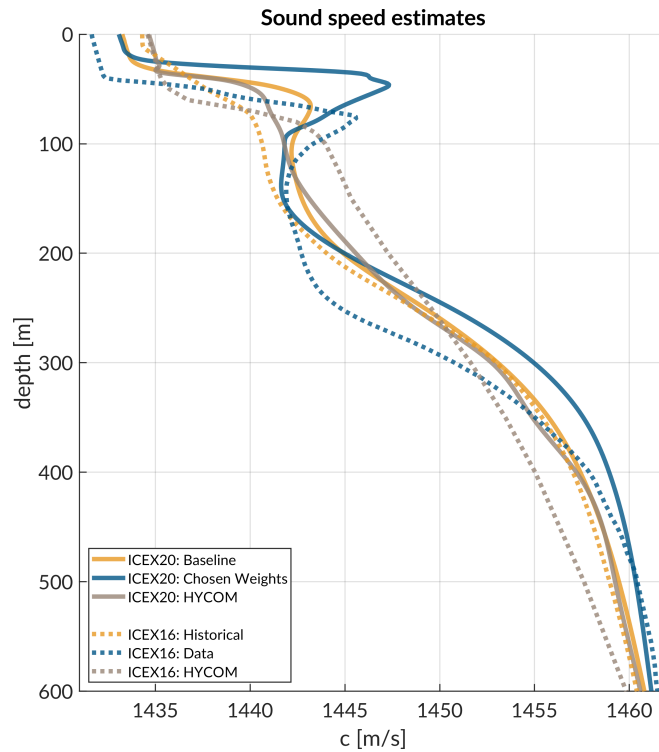


FIG. 3. Sound speed conditions for historical (baseline), data (chosen weights), and HYCOM model for both ICEX16 and ICEX20.

222 **III. REAL-TIME PSEUDORANGE ANALYSIS**

223 Because the vehicle’s navigation solution during a mission can only be evaluated on the
224 basis of the error estimates sent, a sister experiment for validating the real-time ranging
225 approach was implemented. Ice buoy modems were run as “virtual vehicles” at a fixed
226 depth, receiving position updates from the other beacons as well as a camp site modem
227 lowered to 20 m. Figure 4 shows successful events sorted by source depth. In this analysis,
228 we assume there is insignificant displacement between the GNSS puck surface expression
229 and subsurface modem; this is supported by unusually low observed ice drift rates, just 0.7
230 cm/s on average throughout the mission.

231 **A. Minimal bounce criteria (MBC)**

232 The fundamental challenge to implement GNSS-like navigation, especially in an acousti-
233 cally complex propagation environment, is characterizing a single sound speed to compensate
234 for the effects of ray refraction and reflection. The use of the acoustic modem network for
235 tracking relies on the accurate estimates of travel times between the submerged platform
236 and LBL beacons, supported by clock synchronization and a pre-determined scheduling of
237 acoustic events. For the Beaufort Lens in particular, the strong multipath effects make it
238 virtually impossible to deterministically predict the modem’s detected arrival time.

239 Instead, for each individual modem i , an embedded stochastic tracking framework is used
240 to provide a running estimate of the effective sound speed $c_{i,j}$ for the conversion from travel
241 time to range from modem j , with the ultimate goal of matching the implied horizontal

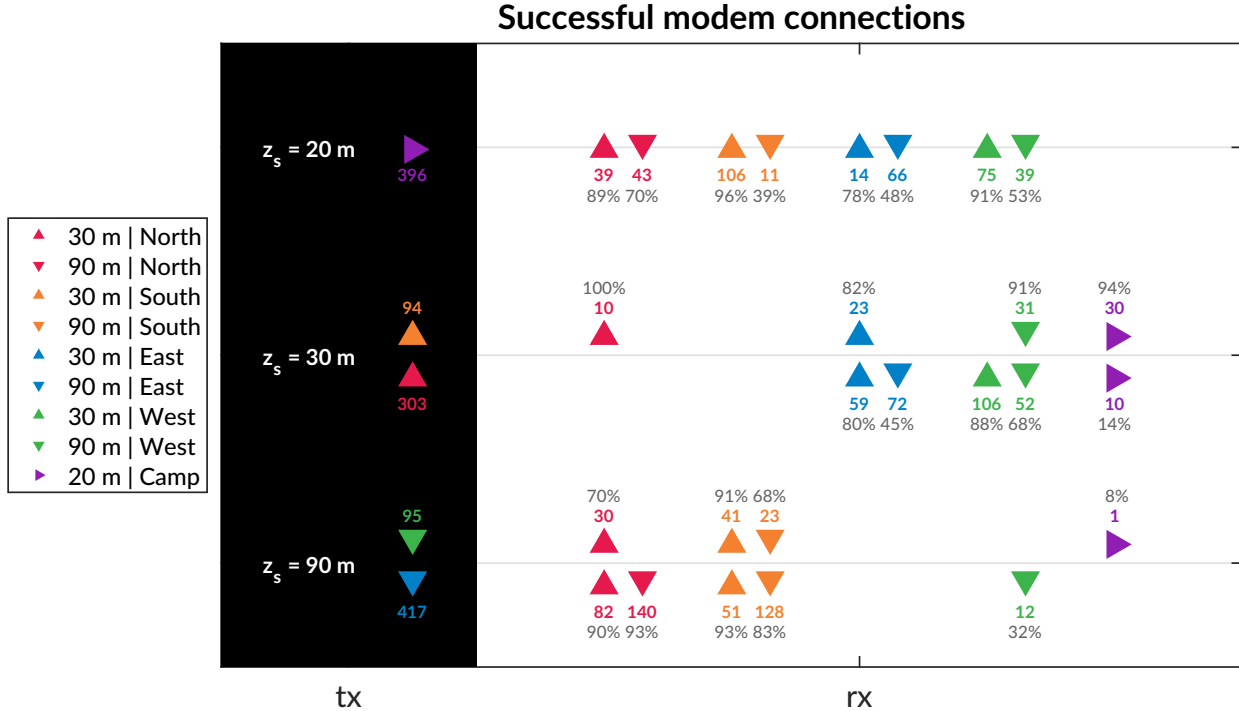


FIG. 4. An overview of the modem experiment by source and receiver depth and position. The black column on the left, *tx*, shows the source depth, z_s , with the total number of transmissions. The column on the right, *rx*, shows the receivers with the number of successful decodings and the percent success rate, defined as the ratio of decoded to detected. The orientation of the triangles—sideways, upwards, and downwards—corresponds to depths of 20, 30, and 90 m.

²⁴² effective sound speed, i.e., the GPS-recorded distance between two nodes divided by the
²⁴³ modem-recorded one way travel time between them.

²⁴⁴ In the ICEX20 configuration, the acoustic tracking is running on the topside computer,
²⁴⁵ which controls the ICNN. Here we assume that the effective sound speeds $c_{i,j}$ are smoothly

²⁴⁶ varying over the course of a vehicle mission, i.e., with respect to range, mission time, and
²⁴⁷ the thirty-second frequency.

²⁴⁸ When the topside tracking framework receives a message, with a time delay, Δt , it will
²⁴⁹ request a new estimate for $c_{i,j}$ along with its standard deviation. The effective sound speed
²⁵⁰ is predicted using the vehicle's reported depth and the extrapolated navigation solution for
²⁵¹ range, \hat{r} , as inputs to the ray tracing program, which returns an impulse response estimate
²⁵² in the form of ray travel times dt_j and amplitudes a_j .

²⁵³ The initial call to BELLHOP is over a local grid centered at the range and depth posited
²⁵⁴ by the onboard tracking solution. The grid, compared to a point solver, adds redundancy
²⁵⁵ in resolving the actual multipath structure for a reliable acoustic path without overtaxing
²⁵⁶ onboard computational time and memory. It is initialized as 11×11 points spanning 10
²⁵⁷ m horizontally and 20 m vertically. The horizontal dimension reflects the accumulated
²⁵⁸ vehicle position error given a thirty-second communication cycle; the vertical dimension
²⁵⁹ reflects how, computationally, eigenrays of the same timefront seem to stack vertically in
²⁶⁰ the water column. For each grid point, BELLHOP produces a number of arrivals resulting
²⁶¹ from multiple propagation paths. Using only the N_0 rays with neither surface nor bottom
²⁶² bounces, it will then estimate the current effective sound speed c from a power weighted
²⁶³ average of the ray travel times,

$$c = \frac{\hat{r} \sum_{n=1}^{N_0} a_n^2}{\sum_{n=1}^{N_0} dt_n a_n^2}, \quad (1)$$

²⁶⁴ and the associated weighted standard deviation,

$$\sigma_c \simeq \sqrt{\frac{\sum_{n=1}^{N_0} (dt_n - \hat{r}/u)^2 a_n^2}{\sum_{n=1}^{N_0} a_n^2}} \frac{u^2}{\hat{r}} \quad (2)$$

²⁶⁵ If no direct paths exist, i.e. $N_0 = 0$, then the effective speed is computed using the same
²⁶⁶ algorithm for the ray arrivals with one bounce, and so on.

²⁶⁷ Finally, the pseudorange is calculated simply as

$$r_{i,j} = c_{i,j} \Delta t_{i,j} \quad (3)$$

²⁶⁸ Thus the MBC method assumes the signal detected by the modem will be dominated by
²⁶⁹ a set of paths with the least number of boundary interactions. Importantly, this stochastic,
²⁷⁰ ensemble method for group velocity calculation can run in real-time, appearing to be orders
²⁷¹ of magnitude faster than other post-processing methods which seek to determine the specific
²⁷² ray itself that best matches a prominent indicator from the arrival structure. The BELLHOP
²⁷³ simulation that runs this calculation uses 3600 rays with launch angle fan of -60 to 60 degrees,
²⁷⁴ a representative depth dependent sound speed profile, and a range dependent bathymetry.

²⁷⁵ B. Pseudorange error metrics

²⁷⁶ The sister modem experiment generated 811 beacon to beacon communication events with
²⁷⁷ their own real-time MBC group velocity predictions. Given the complexity of the ICNN
²⁷⁸ system, this experiment did not collect an exhaustive set of data across all buoy, source
²⁷⁹ depth, receive depth, and sound speed combinations. The algorithm generally overestimates
²⁸⁰ pseudoranges because it resolves the effective sound speed for the most direct path.

²⁸¹ Fig. 5 shows the range error boundary for both SSP inputs used in ICEX20. A promising
²⁸² sign that the MBC method adapts sound speed somewhat intelligently is the lack of error
²⁸³ growth as travel time increases. The baseline SSP ($n=243$ events) has an absolute pseudor-

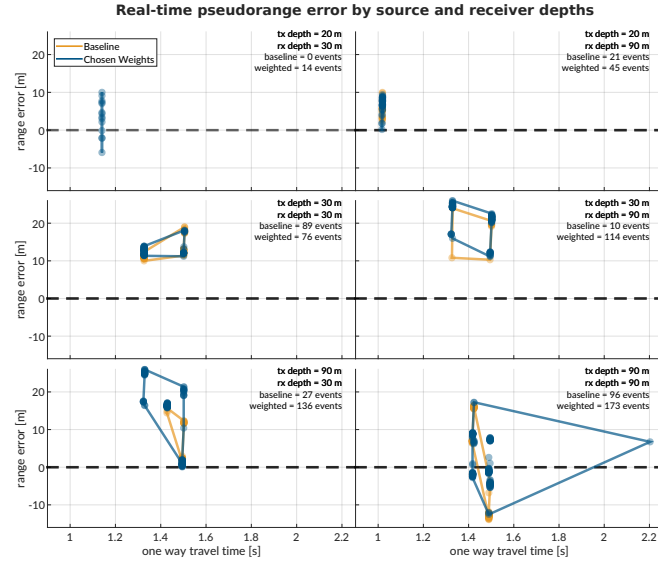


FIG. 5. The real-time range error by source (rows: 20, 30, and 90 m) and receiver (columns: 30 and 90 m) pairings for both sound speed estimates used during ICEX20. The amount of communication events is notated in the top right of each panel. The dashed line indicates no range error, and the boundary drawn indicates scope of the range error as a function of one way travel time.

284 range error of 11.38 ± 4.23 m; the weighted SSP ($n=568$), 11.36 ± 8.12 m. The discrepancy
 285 between these two is largely due to outlier events only contained in the weighted SSP set.
 286 Where there is overlap between sound speed conditions used for the real-time MBC, the
 287 pseudorange error difference is no more than a few meters. The overarching results show
 288 that sound speed estimates derived from eigenrays for a local grid, as opposed to a singular
 289 point, are accurate enough to support vehicle navigation. While the NBC looks for just the
 290 least complex multipath, the high density of launch angles almost always guarantees a direct
 291 path. Nonetheless, the consistent overestimation of pseudorange invites further analysis into
 292 acoustic arrival matching.

293 **C. Eigenray identification for beacon-to-beacon events**

294 Accounting for ice movement between beacons creates nominal ranges with small vari-
 295 ability. Figs. 6, 7, and 8 show eigenrays for three sound speed environments for source
 296 depths of 20, 30, and 90 m, respectively. Eigenrays were initially found using the built-in
 297 BELLHOP protocol with a launch angle fan of 2400 rays between -60 and 60 degrees. Sepa-
 298 rately, recorded travel times between beacons were clustered with 1 millisecond boundaries
 299 such that some source-receiver pairs had multiple, distinct travel times to approximate. The
 300 BELLHOP eigenray returns were then filtered such that one was selected per travel time
 301 cluster, in the hopes that the eigenray will converge to the receiver locations for the most
 302 realistic sound speed input. It should be noted that bottom bounces were recovered but
 303 filtered out. The three source depths create distinct ray geometries with respect to the three
 304 sound speed inputs.

305 **1. Source depth of 20 m**

306 For a source at 20 m in depth, shown in Fig. 6, reliable eigenrays are found for all sound
 307 speed inputs. Rays refract upwards and neatly intersect with the shallow and deep receiver
 308 locations between 1.5 and 1.8 km in range. However, the ray paths for the shallow receivers
 309 change both in the number of surface interactions and where the surface interactions occur
 310 with respect to range across the SSPs. As the Beaufort Lens strengthens, the chosen paths to
 311 the second farthest shallow buoy (North, in red) interact with the surface more and become
 312 distinct. The weighted SSP shows the most interesting effects for the deeper receivers. The

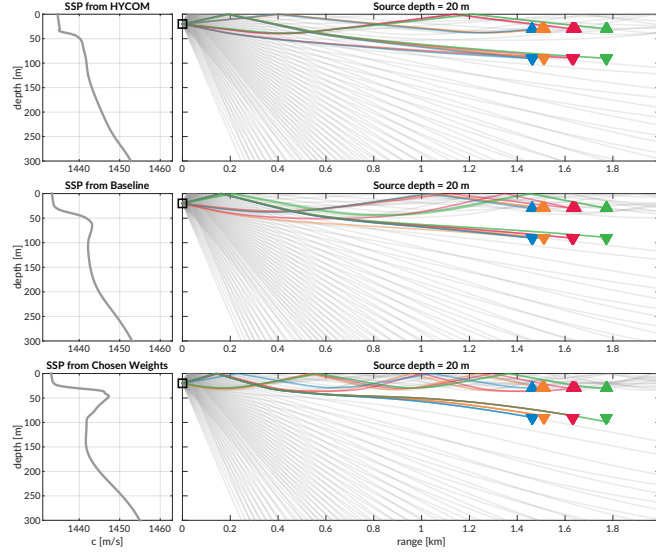


FIG. 6. Eigenrays for beacon-to-beacon events for each sound speed with a nominal source depth of 20 m over a total ray fan in gray. The beacons are highlighted in color/marker coding in Fig. 4.

313 ray paths all interact with the surface and the eigenrays for the Northern (red) and Western
314 (green) buoys are in fact the same ray.

315 2. Source depth of 30 m

316 The ray geometries from the 30 m source, shown in Fig. 6, show a similar degradation
317 of eigenray identification with increased ducting. Receptions span 1.5 to 3.2 km. Once
318 again, eigenrays for HYCOM and the baseline SSP are visually appropriate. Rays for the
319 weighted SSP show how the surface channel intensifies ice interactions and how the shadow
320 zone denies reliable acoustic paths. Pointedly, the increasing number of surface reflections to
321 the farthest shallow buoy (North, in red) crystallize the MBC's tendency for overestimation.
322 For the HYCOM, baseline, and weighted SSP inputs, the most appropriate eigenrays show
323 2, 3, and 4 surface interactions.

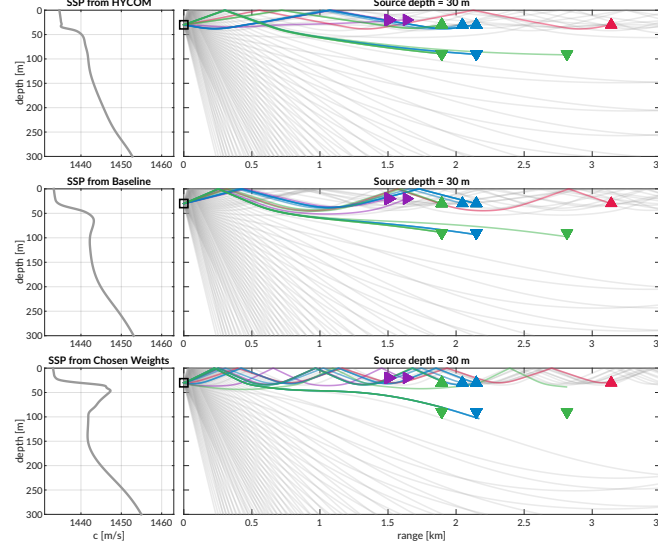


FIG. 7. Eigenrays for beacon-to-beacon events for each sound speed with a nominal source depth of 30 m over a total ray fan in gray. The beacons are highlighted in color/marker coding in Fig. 4.

324

3. Source depth of 90 m

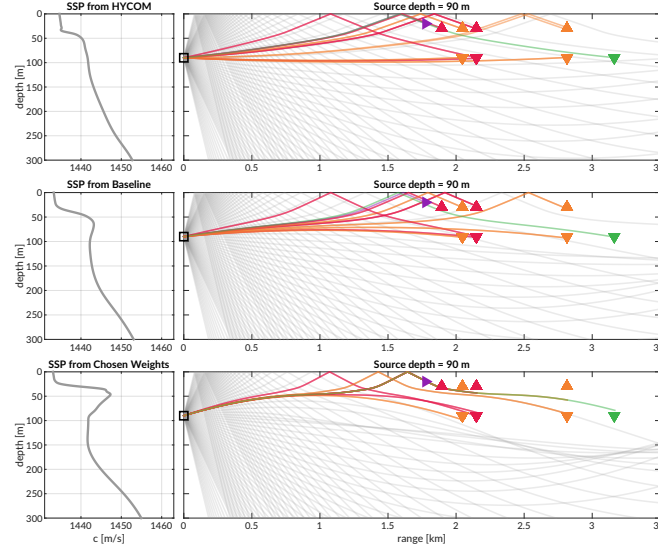


FIG. 8. Eigenrays for beacon-to-beacon events for each sound speed with a nominal source depth of 90 m over a total ray fan in gray. The beacons are highlighted in color/marker coding in Fig. 4.

325 Lastly, Fig. 8 shows ray geometries from the 90 m source, elucidating a different extent
326 of the shadow zone. While the receiver locations are similar to that of the 30 m source
327 depth, the deeper source depth effectively negates the upper duct and places the upper (and
328 some of the lower) receivers in unreliable acoustic paths. The HYCOM eigenrays still show
329 the most reliable acoustic paths that deteriorate with increasing ducted conditions. The
330 lack of direct paths from the observed SSP further points out the shortcomings of the MBC
331 approach.

332 The goal of the MBC algorithm was to provide a reliable, physically intuitive interpre-
333 tation of the acoustic propagation without taking on the additional burden of regularly
334 identifying specific paths that may connect any given source-receiver pair in the network.
335 While it was unlikely to resolve multipath arrivals that triggered successful modem detec-
336 tion, an isovelocity approach would have provided no adaptivity against source and receiver
337 depth differences. Its performance was adequate for vehicle navigation and would have likely
338 sufficed if it were not for the prominence of the duct observed relative that of other model
339 and data products.

³⁴⁰ **IV. POST-PROCESSED PSEUDORANGE ANALYSIS**

³⁴¹ From all events recorded during the modem test experiment, there are 1242 successfully
³⁴² decoded beacon-to-beacon events. Thus, a post-processing analysis that emulates the real-
³⁴³ time navigation engine was run to overcome the unequal distribution of communication
³⁴⁴ events with respect to depth, range, and sound speed status.

³⁴⁵ It is important to note that the value for the extrapolated range, \hat{r} , is only tracked when
³⁴⁶ the modem runs the vehicle behavior; thus we replace \hat{r} with the GPS-tracked range for
³⁴⁷ all modem events. Because \hat{r} converges to the correct solution, a comparison of \hat{r} with the
³⁴⁸ GPS-tracked range shows a normal, zero-centered distribution within the bounds of GPS
³⁴⁹ drift. The analysis therefore seeds realistic but “omniscient” knowledge of the extrapolated
³⁵⁰ range and emulates the post-processing pipeline to more thoroughly evaluate the acoustic
³⁵¹ pseudorange estimate for all modem events. Sound speed inputs are the isovelocity sound
³⁵² speed in addition to the modeled, baseline, and weighted SSPs from Fig. 3. The analysis
³⁵³ replicates the MBC but also introduces a new filtering algorithm, the nearest bounce criteria
³⁵⁴ (NBC), based on insights gleaned from the eigenray analysis. Accordingly, the results in
³⁵⁵ this section evaluate the utility of the algorithms and sound speed sources, divorced from
³⁵⁶ their role in the ICNN while maintaining real-time relevance.

³⁵⁷ **A. Nearest bounce criteria (NBC)**

³⁵⁸ The extent of ray bending and repeated reflections is extremely dependent on the degree
³⁵⁹ of the Beaufort Lens observed. Based on this insight, a new algorithm, the nearest bounce

³⁶⁰ criteria (NBC), is a slight modification from the MBC and includes multipath as a new
³⁶¹ dimension of information to exploit. This metric, while run in post-processing, adds a
³⁶² negligible amount of computation for real-time efficacy.

³⁶³ Given a running estimate for the effective sound speed $c_{i,j}$ between nodes i and j , the
³⁶⁴ navigation system has an extrapolated value for range, \hat{r} , and a recorded travel time, $\Delta t_{i,j}$.
³⁶⁵ Instead of using only the N_0 rays with neither surface nor bottom bounces to estimate
³⁶⁶ conversion speed, and subsequently moving to incremental number of bounces only when no
³⁶⁷ valid direct path solutions exist, we solve for the power weighted average of the ray travel
³⁶⁸ time for the N_k rays with k bounces,

$$t_k = \frac{\sum_{n=1}^{N_k} dt_n a_n^2}{\sum_{n=1}^{N_k} a_n^2}, \quad (4)$$

³⁶⁹ find the nearest matching power weighted average to recorded travel time,

$$t_{i,j,k} = \min_{k=0,1,2,\dots} |t_k - \Delta t_{i,j}| \quad (5)$$

³⁷⁰ predict an effective sound speed,

$$c_{i,j} = \frac{\hat{r}}{t_{i,j,k}} \quad (6)$$

³⁷¹ and estimate the range as was done previously.

$$r_{i,j} = c_{i,j} \Delta t_{i,j} \quad (7)$$

³⁷² This method selects a different effective sound speed based on the multipath arrival struc-
³⁷³ ture, as the detected arrival is not always the first arrival or the direct path and could even
³⁷⁴ be masked by noise or blocked temporarily (Deffenbaugh *et al.*, 1996b). We manually cap

375 the number of bounces at four because of the smaller operational scale and the attenua-
 376 tion accrued with many surface interactions. Bottom bounces are not encoded separately
 377 because of ray's tendency to refract upward, not due to information limitations.

378 **B. Effective sound speed predictions**

379 The minimal and nearest bounce algorithms are applied with the three sound speed inputs
 380 shown in Figs. 6, 7, 8. The resulting predicted effective sound speeds are shown in Fig. 9
 381 for all source depths versus one way travel time.

382 The goal of the effective sound speed prediction is to converge towards the implied sound
 383 speed, i.e. the GNSS-derived range divided by the recorded travel time. As the environ-
 384 mental and ray filtering method become better representations of the real ocean, the lower
 385 the expected mismatch is between the implied and estimated effective sound speeds.

386 The various sound speed inputs—isovelocity aside—not only modify the predicted effec-
 387 tive sound speed, as seen by the colored vertical offsets, but often classify a distinct number
 388 of bounces. HYCOM sees the most direct and one bounce multipath structures, lending a
 389 bias for faster speeds; the weighted SSP sees the most double and triple bounces, favoring
 390 slower speeds; the baseline sound speed exists in between. Very rarely is the multipath
 391 structure classified as a direct path, where the MBC and NBC would prediction overlap. In
 392 fact, the higher the multipath classification, the more accurate the sound speed prediction
 393 is, likely driven by a tighter or even sparser bundle of rays. Discontinuities in multipath
 394 classification provide initial evidence for its importance to a smoothly varying group veloc-
 395 ity, as shown in the cluster of 30 to 30 m transmissions, where HYCOM jumps from one to

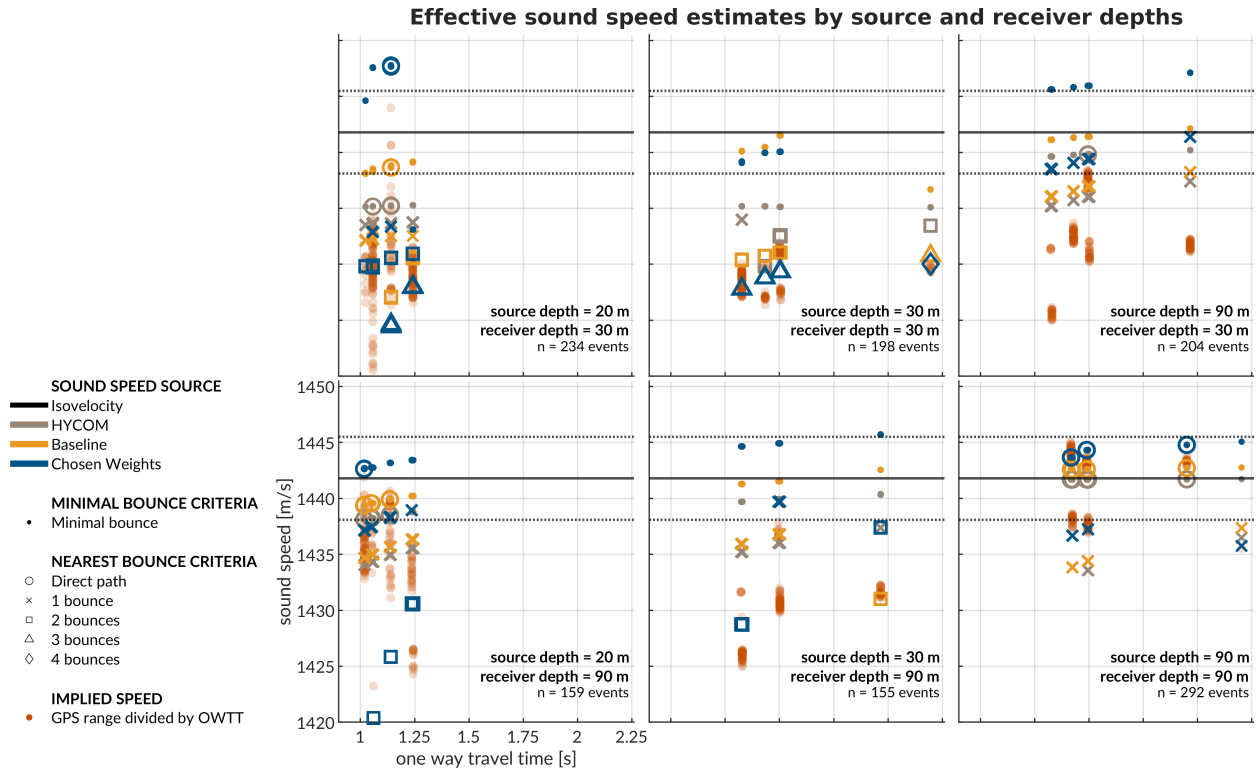


FIG. 9. A post-processing comparison of effective sound speed predictions for all beacon-to-beacon events. The rows share receiver depth; the columns share source depth. The recorded travel time is on the x-axis and the predicted effective sound speed is on the y-axis. The sound speed source is indicated by color. The isovelocity is shown as the mean \pm the standard deviation. The minimal and nearest bounce criterion are distinguished by different marker shapes, compared to the separately colored red dots showing the implied calculation.

396 two classified bounces amidst the baseline SSP and weighted SSP smoothly increasing while
 397 consistently seeing two and three classified bounces, respectively. Of course, the prediction
 398 deteriorates with cross-layer transmissions across the duct, but not to the same degree at
 399 which eigenrays could not be found for the weighted SSP in section III C. The evidence sug-

400 gests that the grid based method provides a useful amount of redundancy to resolve similar
 401 enough eigenrays.

402 It is useful to think about in what case the isovelocity—or any isovelocity framing—would
 403 have been appropriate. The transmissions from shallow to shallow receiver would may have
 404 matched the default configuration of 1430 m/s. The isovelocity contrived for this paper,
 405 1441.8 m/s, best matches the transmissions from 90 to 90 m. The one from [Graupe *et al.*](#)
 406 ([2019](#)), 1450 m/s, would have had a systemic overestimation. Given that implied sound
 407 speeds just for beacon-to-beacon events span 1420 to 1445 m/s, it is safe to say that a
 408 nominal sound speed would sacrifice pseudorange accuracy somewhere, and that an adaptive
 409 approach is necessary even for short range operations in the Beaufort Lens.

410 **C. Pseudorange error metrics**

411 Pseudorange estimation plays an important role in trilateration. Fig. [10](#) shows the
 412 directional pseudorange error “footprints” for the four sound speed inputs with the NBC
 413 approach, separated by source and receiver depth configurations.

414 The weighted SSP range error generally has the smallest and most zero-centered footprint.
 415 The one case it does not is for the source-receiver pairings between 30 and 90 m in depth. The
 416 increased error for these is most likely driven by the computational artifacts encountered
 417 when propagating through the steep sound speed gradients of the lens and through the
 418 shadow zone. All other source depth pairings are significantly improved using the chosen
 419 weights compared to HYCOM or the baseline.

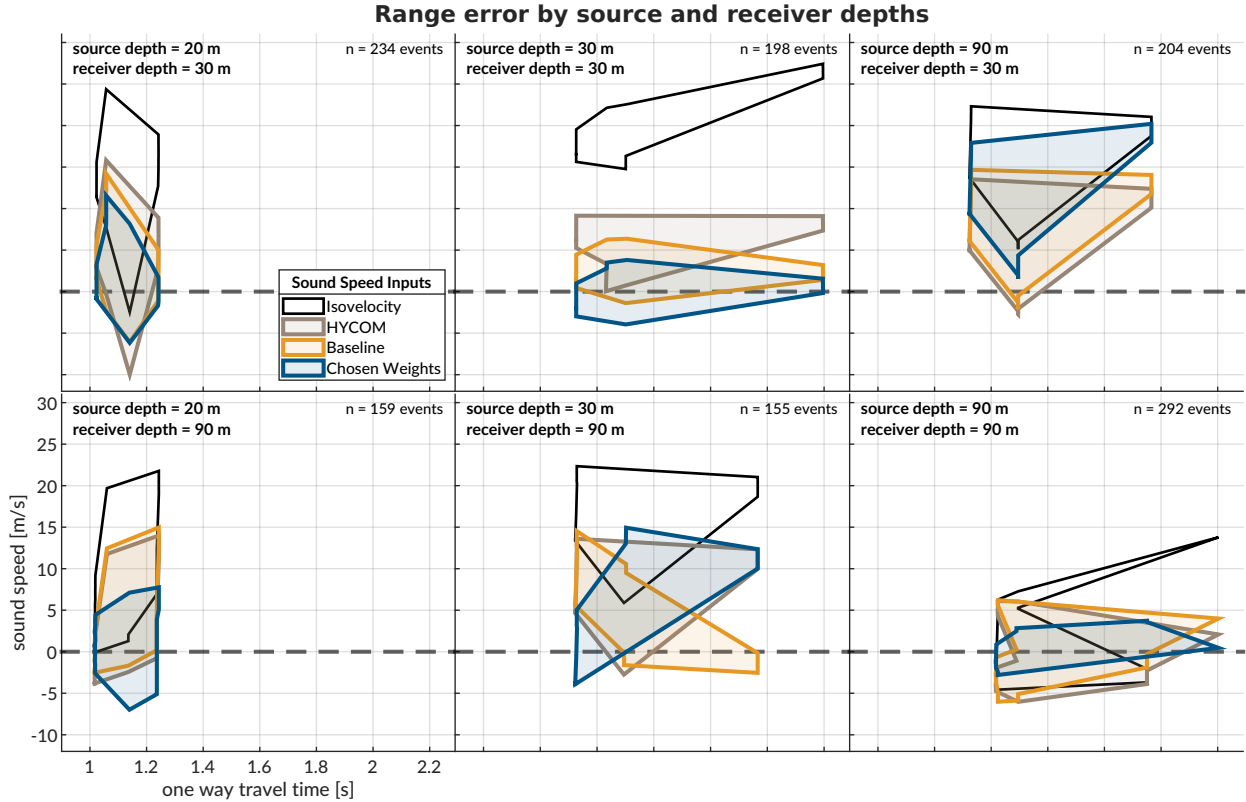


FIG. 10. The post-processed pseudorange error; the rows share receiver depth; the columns share source depth. The dashed gray line shows no error. The shaded region connects the range performance across all events.

When using a linear scaling to convert travel time into range, any offset between the assumed sound speed and the horizontal group velocity produces unconstrained error with increasing receiver distance, whereas an adaptive estimate would exhibit no such trend. This is easily observed in the same-layer links, i.e., 30 to 30 m and 90 to 90 m. In cross-layer links, the isovelocity does not perform better but tends to exaggerate or flip the footprint created adaptively.

The improvement from MBC to NBC is most evident for the data-driven sound speed; while the HYCOM SSP improves from a median absolute range error of 6.41 to 4.61 m,

428 the baseline SSP improves from 10.30 to 2.27 m, and the weighted SSP improves from
429 13.28 to 2.12 m. In comparison, the isovelocity has a median error of 13.09 m. The order
430 of magnitude improvement in the ducted SSPs demonstrate the effectiveness of the NBC
431 algorithm exploiting the observed multipath conditions.

432 There is one example that helpfully illustrates the improvement brought upon by bounce
433 classification. For transmissions between North and South at 30 m, the OWTT spread
434 is 2.1958 to 2.1963; the GNSS-tracked distance is 3138.54 to 3140.87 m; and the implied
435 effective sound speed is 1429.3 to 1430.1 m/s. For these transmissions, the weighted SSP
436 and the MBC approach produce a pseudorange error of -1491 m, as the effective sound speed
437 is dominated by bottom bounce arrivals with much greater travel times. The NBC approach
438 categorizes this same record as a quadruple surface bounce, reducing the pseudorange error
439 to less than a meter. Comparatively, the NBC approach for HYCOM and the baseline
440 SSP produce pseudorange errors of 8.30 and 2.39 m, respectively. There is strong evidence
441 to suggest that the sound speed and multipath fidelity codependently improve localization
442 accuracy.

⁴⁴³ **V. TRILATERATION FOR ICEX20 FIELD DATA**

⁴⁴⁴ To overcome potentially intermittent acoustic communication, the operational paradigm
⁴⁴⁵ of the ICNN computes corrections relative to the trilaterated position estimates transmitted
⁴⁴⁶ by the vehicle, rather than transmitting the updated positions themselves. The reliability
⁴⁴⁷ of the correction is directly linked to how accurately the travel time measurements are
⁴⁴⁸ converted to pseudoranges. This section aims to resolve that tension by reevaluating the
⁴⁴⁹ trilateration results with respect to the MBC and NBC algorithms. The MBC/NBC sound
⁴⁵⁰ speed estimates were tracked independently for each transmitter-receiver pair; although the
⁴⁵¹ sound speed was expected to be locally smooth near a given receiver, no such assumption
⁴⁵² was enforced between distinct acoustic links.

⁴⁵³ **A. Re-positioning beacon to beacon events**

⁴⁵⁴ When the beacons ran as virtual vehicles, the ICNN did not have access to that buoy's
⁴⁵⁵ GPS data stream except for what was sent via digital acoustic message. The static nature of
⁴⁵⁶ the experiment means that the initial estimate transmitted to the ICNN was in fact a ground
⁴⁵⁷ truth position. Therefore, a distribution of corrections from the ICNN, as shown in Fig. 11,
⁴⁵⁸ reflects positioning accuracy. The NBC clearly outperforms the MBC, with almost 80% of
⁴⁵⁹ the corrections below 6 meters and the median within the deployed GNSS puck precision
⁴⁶⁰ of 3 meters. By contrast, the MBC shows roughly 20% within the GNSS puck precision,
⁴⁶¹ and separate peaks from 9–12 meters and 21–27 meters. This trimodal nature reflects the
⁴⁶² distribution of reflections on the ice surface.

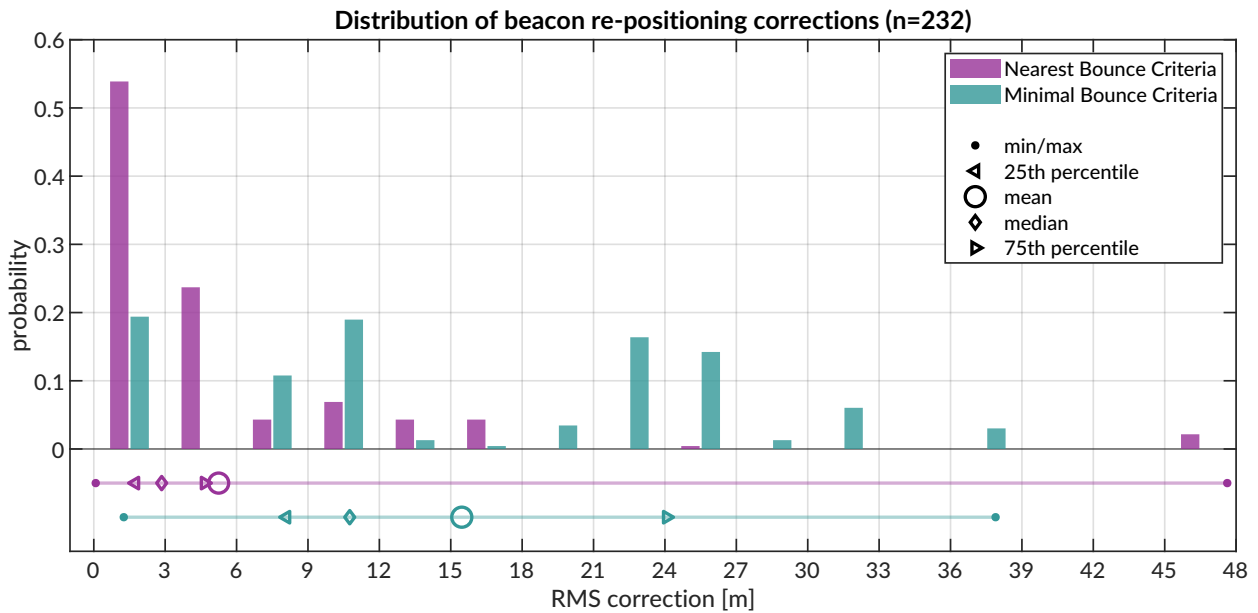


FIG. 11. Trilateration events; however, 264 entries are 2-beacon solutions, 22 are 3-beacon, and 2 are 4-beacon. When limited to only two ranging circles, the trilateration chooses the closer of the two intersection points. The x-axis is cut off at the upper limit for the NBC algorithm.

463 In several events, the MBC is unable to accurately estimate the effective sound speed for
 464 one of the acoustic links, leading to a large positioning error. The NBC, however, better
 465 resolves an approximation of the acoustic path. For example, in some trilateration solutions
 466 for the Eastern buoy, the MBC shows a correction of more than a kilometer; the NBC is
 467 two order of magnitudes less.

468 **B. Re-navigating AUV *Macrura***

469 Up to this point, pseudorange estimation and localization have been evaluated on GPS-
 470 linked beacon-to-beacon connections to validate the NBC algorithm. This analysis ports the
 471 MBC and NBC algorithms to re-navigate the AUV *Macrura*.

472 The AUV dataset clearly exhibits instances where a receiver detects the same transmission
 473 more than once. This is not surprising considering the complex multipath provided by
 474 the Beaufort Lens. The 11 hour vehicle mission contains 3260 transmissions, 12938 total
 475 detections, and 4704 successful receptions. Allowing receptions with PSK errors would
 476 almost double the number of recorded multipath arrivals exploited for positioning, if a real-
 477 time solution could correctly parse paths from different arrivals in the same thirty-second
 478 cycle. Thus it remains a future endeavor to explore how failure mode information from
 479 acoustic modems could be used to identify unsuccessful but otherwise trustworthy arrivals
 480 to augment trilateration samples.

481 The following performance analysis is constrained to what the vehicle acted on in real-
 482 time. AUV *Macrura* and the ICNN ran an adaptive depth behavior to maintain acoustic
 483 communication on the insight that cross-layer links were more likely to fail than same-layer
 484 ones. Accordingly, the vehicle dove deeper than 50 meters about 20% of the time it was
 485 underway.

486 In contrast to the modem tests, where position correction illustrated re-positioning ac-
 487 curacy, the re-navigation corrections are less valuable in the absence of GNSS ground truth.
 488 The correction magnitude necessarily depends on the vehicle's internal navigation estimate,
 489 which is prone to larger errors from sensor drifts, ocean currents, and other error not cap-
 490 tured in the hydrodynamic model. Thus, larger corrections are not necessarily indicative of
 491 worse performance. Navigation accuracy may be better described by trilateration error, the
 492 RMS of the remaining pseudorange errors from each acoustic link.

493 Fig. 12 shows the correction magnitudes and trilateration errors for events with three or
 494 more receptions during AUV operations. Whereas the MBC has a fairly bimodal nature,
 495 with peaks centered around 10–15 and 35–40 m, the NBC favors smaller corrections, from
 496 5–20 m, and has a long tail. The distribution of corrections are much larger than the
 497 distribution of RMS error. It is apparent that, while both methods are quite successful,
 498 there is strong evidence that the NBC achieves single meter accuracy.

499 **C. Investigating potential GNSS noise**

500 The fact that the bulk of the best performing re-navigation error exists within the pre-
 501 cision of the GNSS unit deployed invites a further look into GNSS noise. In the Arctic,
 502 GNSS performance worsens due to poor constellation coverage, larger ionospheric effects,
 503 and multipath interference. The National Security Implications of Climate Change for U.S.
 504 Naval Forces (Council, 2011) details some of the limitations of the Global Positioning Sys-
 505 tem (GPS) at polar latitudes. Radio infrastructure that provides position corrections and
 506 references does not regularly extend to polar regions. The effect is minor for surface platform
 507 navigation —roughly 15 m of horizontal precision has been displayed at the North Pole—but
 508 is significant enough to register against the modem’s detected travel times. Figure 13 zooms
 509 in on the GNSS and OWTT noise relative to the ice movement for two pairs of modem buoy
 510 connections. The two panels indicate the GPS drift as $\delta R = \sqrt{\delta x^2 + \delta y^2}$ and temporal drift,
 511 δt , relative to the median OWTT recorded between the two modems. The dashed line is
 512 scaled by a group velocity of 1440 m/s, such that if there were ideal sensor measurements
 513 with no drift, all events should exist on or near the line.

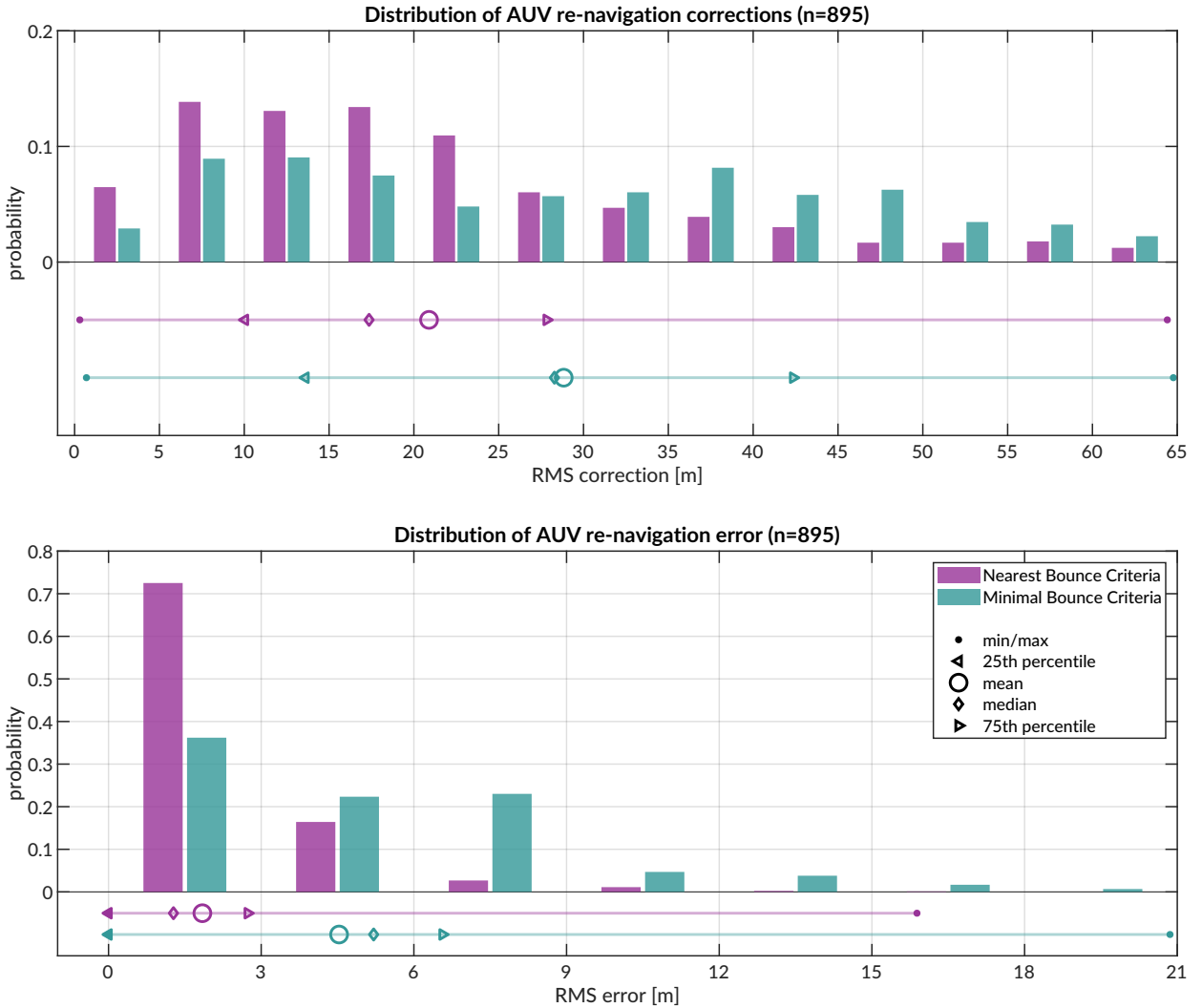


FIG. 12. Distribution of vehicle re-navigation corrections (top) and error (bottom) computed in post-processing for the Minimum and Nearest Bounce Criterion.

514 The top panel shows the connections between the North and East buoys. There is relative, i.e. non-rigid, ice movement between the North and East buoys, evidenced by events spanning the dashed line. But the height of the scatter plot is indicative of the precision of the GPS signal, as it remains consistent across many arrival time bands. Naturally, some minor offsets between these vertical bands relate to different operational configurations of

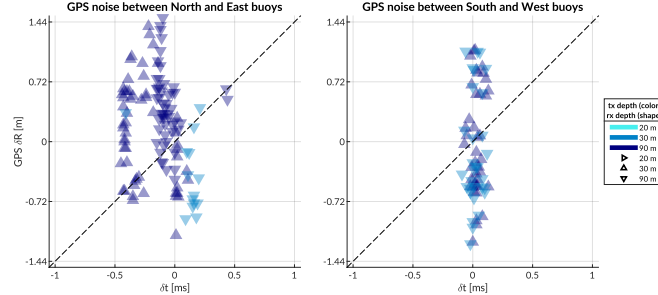


FIG. 13. A comparison of GPS drift (y-axis) versus OWTT drift (x-axis), colored by source and receiver depth. The physical link between North and East are shown on the top; South and West is on the bottom.

519 source and receiver depth. However, the large majority of events show vertical banding for
 520 the same nominal δt , indicating the amount of GPS drift.

521 This idea of GPS drift relative to the same OWTT measurements is further indicated by
 522 events between the other two buoys, South and West, in the bottom panel. These buoys are
 523 moving in a more rigid ice floe and there is minimal impact by source and receiver depth
 524 on the spread of OWTT. The GPS drift is much larger relative to the OWTT drift, which
 525 is sensitive to acoustic scattering, multipath, and/or environmental microstructure.

526 These are just two subsets of the physical links that cover all four GPS modem buoys. The
 527 GPS at camp is the least accurate due to the human activity and infrastructure occluding
 528 the physical puck.

529 VI. DISCUSSION

530 Given the computational constraints of real-time modeling, the gridded approach facil-
 531 itates enough multipath classification to build in a “ray ensemble” of characteristic group

532 velocities. This result is not always possible when aiming to find eigenrays to just an individual point, even with a higher density of launch angles. An important takeaway for those
 533 interested in ray-based localization is leveraging a local grid to give BELLHOP tolerance
 534 for finding solutions that otherwise may not be found in a center or single point solution.
 535 The limitations of numerical computation, particularly for a complex environment, are more
 536 adeptly addressed by accepting some uncertainty in position than by prescribing an exact
 537 solution. Even though BELLHOP is a greedy estimator for eigenrays, the additional data
 538 created is a negligible burden.

540 Underwater navigation research is broadly motivated by acquiring GPS-like navigation
 541 accuracy in GPS-denied conditions. The Arctic, while remote, is the perfect place to test
 542 mature navigation technologies in real GPS-denied conditions.

543 Range estimation is an essential step of acoustic localization and navigation. Current
 544 approaches in real-time underwater acoustic navigation simplify the non-linear relationship
 545 between a sound speed profile and acoustic propagation with a deterministic sound speed.
 546 Some post-processing approaches attempt to leverage the acoustic arrival structure via var-
 547 ious ray methods, but often use a singular SSP for simplicity, even over long term missions
 548 or dynamic conditions. Thus, the conversion from travel time to range, particularly for
 549 real-time vehicle deployments, can be pre-conditioned for error growth as the OWTT/range
 550 increases.

551 For GPS-denied navigation, especially in hostile environments like the Arctic, tolerance
 552 for error is close to none. This work addresses a critical need in acoustic navigation by

553 retooling acoustic arrival methods generally deemed too complex or labor intensive for real-
 554 time, ray-based range estimation to achieve GPS-like positioning.

555 We hypothesize and validate that the embedded stochastic prediction of a single group
 556 velocity is a smoothly varying function of range, source and receiver depth pairings, as
 557 well as multipath structure. We employ a GPS-tracked experiment to have a ground truth
 558 comparison for real-time localization algorithms. The real-time system achieves GPS-like
 559 navigation for an AUV without taking into account multipath structure; the ranging error
 560 improves by an order of magnitude with the suggested multipath adaptability, minimizing
 561 range error to single meters. Post-processing analysis shows that this method of ranging is
 562 sensitive to GPS drift itself; thus embedding a stochastic prediction of the horizontal group
 563 velocity has an outsized benefit to minimizing trilateration error.

564 There are many avenues through which this approach can be further refined and tested for
 565 field operations. Amongst them is defining the uncertainty grid for BELLHOP via stochastic
 566 or data-driven measures such as the distance traveled by the AUV between ICNN updates
 567 or the magnitude of the position corrections by the ICNN. Another is to entirely remove the
 568 seeded range and instead rely on the submerged asset's depth and recorded OWTT to find
 569 high probability fields in range.

570 The literature in underwater acoustic navigation and positioning is either real-time or
 571 physics-based. In this paper we demonstrate a field-tested approach that is both real-time
 572 and physics-based; this is achieved by coupling data streams with fast acoustic modeling.
 573 The methods exploit the upward refracting nature and the total ice cover of the Arctic
 574 environment to achieve remarkable ranging accuracy and precision. It transforms multipath,

575 widely considered as an obstacle for acoustic ranging, into a new information content to
 576 refine ranging accuracy. We believe that this work enables more accurate range estimation,
 577 localization, and/or navigation for any field experiment given known source and receiver
 578 depths.

579 Performance in other acoustic environments may require introducing a different thresh-
 580 olded metric to sort time of arrivals. Given the NBC algorithm's improvement with increased
 581 multipath, its effectiveness is likely only challenged by the valid operational scales of a range
 582 independent propagation environment. For mesoscale operations, like that of many glid-
 583 ers, the group velocity criteria may need to be modified to better account for variability
 584 driven by range dependent propagation through internal waves, eddies, or even bathymetric
 585 changes like underwater volcanoes. BELLHOP simulations provide other relevant eigenray
 586 information, like time and angle of arrival, that is ripe for statistical and machine learning
 587 methods to classify a representative group velocity. A bespoke and fast ray tracing method,
 588 which was used during ICEX20 to evaluate the acoustic fit of sound speed profile parame-
 589 terization ([Bhatt et al., 2022](#)), can easily report back the number of turning points instead
 590 of the number of bounces for multipath classification.

591 This approach will start to break down in extremely dynamic environments, like fast
 592 moving fronts. Realistic *in situ* considerations of the acoustic environment may not be pos-
 593 sible without complete through-the-sensor integration of acoustic dat and/or hyper realistic
 594 ocean models.

595 Many approaches to underwater navigation combine it with acoustic tomography, i.e.,
 596 a joint estimation of both source and receiver locations and the ocean volume between

597 them. There has been considerable success at this effort in post-processing methods,
598 which utilize intensive—and due to the non-linearity of sound propagation, often brute
599 force—computational methods. For vehicle operations, fast tomography is the ideal im-
600 plementation, in that one can fully consider how sound speed structure, horizontally and
601 vertically, influences sound propagation. AUVs can serve as moving sources to better image
602 the ocean volume (Deffenbaugh, 1997; Elisseeff *et al.*, 2002), where mobile tomography and
603 navigation converge on the same set of component technologies: position estimation, sound
604 speed parameterization estimation, ray path identification, and vehicle path optimization.

605 But there are overwhelming challenges, operationally and computationally, for fast, mo-
606 bile tomography to become a realistic endeavor. Addressing the spatial and temporal scales
607 of what can be solved deterministically and what must be solved stochastically imposes a
608 resolution constraint on the utility of gridded models—resolving fine features inaccurately
609 (or with a false sense of confidence) could be more harmful than assuming range indepen-
610 dence. Given that AUV operations are often on small spatial and temporal scales, the added
611 benefit of a gridded model is quite small, and in cases like the Arctic, may actually mis-
612 characterize the ocean volume. For gliders, with longer and larger operational scales, an
613 ocean model may provide more useful information. Currently gliders are low power and do
614 not have the storage or computational power to run a full-scale, realistic ocean model. A
615 lightweight representation of the key environmental and acoustic features, passed through
616 the same manner of acoustic message from the modem experiment, may drastically improve
617 glider navigation.

618 **ACKNOWLEDGMENTS**

619 We acknowledge the significant operational effort spearheaded by the LAMSS ICEX20
 620 team and all our collaborators. Bhatt was funded by a National Defense, Science, and
 621 Engineering Graduate Fellowship. This work was supported by the Office of Naval Research
 622 322-OA under ICEX20 (N00014-17-1-2474) and Task Force Ocean (N00014-19-1-2716).

623

624 Ballard, M. S., Badiey, M., Sagers, J. D., Colosi, J. A., Turgut, A., Pecknold, S., Lin, Y.-T.,
 625 Proshutinsky, A., Krishfield, R., Worcester, P. F., and Dzieciuch, M. A. (**2020**). “Tem-
 626 poral and spatial dependence of a yearlong record of sound propagation from the Canada
 627 Basin to the Chukchi Shelf,” The Journal of the Acoustical Society of America **148**(3),
 628 1663–1680, <http://asa.scitation.org/doi/10.1121/10.0001970http://files/814/>
 629 [Ballardetal.-2020-Temporalandspatialdependenceofayearlongreco.pdf](#), doi: [10.](https://doi.org/10.1121/10.0001970)
 630 [1121/10.0001970](https://doi.org/10.1121/10.0001970).

631 Barker, L. D. L., Jakuba, M. V., Bowen, A. D., German, C. R., Maksym, T., Mayer,
 632 L., Boetius, A., Dutrieux, P., and Whitcomb, L. L. (**2020**). “Scientific challenges and
 633 present capabilities in underwater robotic vehicle design and navigation for oceanographic
 634 exploration under-ice,” Remote Sensing **12**(16), 1–31, doi: [10.3390/RS12162588](https://doi.org/10.3390/RS12162588).

635 Bellingham, J., Leonard, J., Vaganay, J., Goudey, C., Atwood, D., Consi, T., Bales, J.,
 636 Schmidt, H., and Chryssostomidis, C. (**1995**). “Auv operations in the arctic,” in *Sea Ice
 637 Mechanics and Arctic Modeling Workshop*.

- 638 Bhatt, E. C. (2021). “A Virtual Ocean framework for environmentally adaptive, em-
 639 bedded acoustic navigation on autonomous underwater vehicles,” Ph.D. thesis, Mas-
 640 sachusetts Institute of Technology and Woods Hole Oceanographic Institution Joint Pro-
 641 gram, <https://hdl.handle.net/1912/27309>, doi: [10.1575/1912/27309](https://doi.org/10.1575/1912/27309).
- 642 Bhatt, E. C., Howard, B., and Schmidt, H. (2022). “An Embedded Tactical Decision Aid
 643 Framework for Environmentally Adaptive Autonomous Underwater Vehicle Communica-
 644 tion and Navigation,” IEEE Journal of Oceanic Engineering .
- 645 Brooke, J. (1981). “Arcs (autonomous remotely controlled submersible),” in *Proceedings of*
 646 *the 1981 2nd International Symposium on Unmanned Untethered Submersible Technology*,
 647 IEEE, Vol. 2, pp. 28–28.
- 648 Chassignet, E. P., Hurlburt, H. E., Smedstad, O. M., Halliwell, G. R., Hogan, P. J., Wall-
 649 craft, A. J., Baraille, R., and Bleck, R. (2007). “The HYCOM (HYbrid Coordinate
 650 Ocean Model) data assimilative system,” Journal of Marine Systems **65**(1-4), 60–83, doi:
 651 [10.1016/J.JMARSYS.2005.09.016](https://doi.org/10.1016/J.JMARSYS.2005.09.016).
- 652 Chen, R., Poulsen, A., and Schmidt, H. (2019). “Spectral, spatial, and tem-
 653 poral characteristics of underwater ambient noise in the Beaufort Sea in 1994
 654 and 2016,” The Journal of the Acoustical Society of America **145**(2), 605–
 655 614, <https://asa.scitation.org/doi/full/10.1121/1.5088601http://files/757/>
 656 [Chenetal.-2019-Spectral,spatial,andspacecharacteristicsof.pdf](https://files/757/Chenetal.-2019-Spectral,spatial,andspacecharacteristicsof.pdf), doi: 10.
 657 [1121/1.5088601](https://doi.org/10.1121/1.5088601).
- 658 Chen, R., and Schmidt, H. (2020). “Temporal and spatial charac-
 659 teristics of the Beaufort Sea ambient noise environment,” The Jour-

- 660 nal of the Acoustical Society of America **148**(6), 3928–3941, <https://doi.org/10.1121/10.0002955>
- 661 //asa.scitation.org/doi/full/10.1121/10.0002955http://files/755/
- 662 [ChenandSchmidt-2020-TemporalandspatialcharacteristicsoftheBeaufou.pdf](#), doi:
- 663 [10.1121/10.0002955](https://doi.org/10.1121/10.0002955).
- 664 Claus, B., Kepper, J. H., Suman, S., and Kinsey, J. C. (2018). “Closed-loop one-way-travel-
- 665 time navigation using low-grade odometry for autonomous underwater vehicles,” Journal
- 666 of Field Robotics **35**(4), 421–434, doi: [10.1002/rob.21746](https://doi.org/10.1002/rob.21746).
- 667 Council, N. R. (2011). *National Security Implications of Climate Change for U.S. Naval Forces* (The National Academies Press, Washington, DC), <https://www.nap.edu/catalog/12914/national-security-implications-of-climate-change-for-us-naval-forces>.
- 671 Deffenbaugh, M. (1997). “Optimal Ocean Acoustic Tomography and Navigation with Moving Sources,” Ph.D. thesis, MIT-WHOI Joint Program in Oceanography/Applied Ocean
- 672 Science and Engineering.
- 674 Deffenbaugh, M., Bellingham, J. G., and Schmidt, H. (1996a). “Relationship between
- 675 spherical and hyperbolic positioning,” Oceans Conference Record (IEEE) **2**, 590–595, doi:
- 676 [10.1109/OCEANS.1996.568293](https://doi.org/10.1109/OCEANS.1996.568293).
- 677 Deffenbaugh, M., Schmidt, H., and Bellingham, J. G. (1996b). “Acoustic positioning in a
- 678 fading multipath environment,” in *OCEANS 96 MTS/IEEE Conference Proceedings. The*
- 679 *Coastal Ocean-Prospects for the 21st Century*, IEEE, Vol. 2, pp. 596–600.
- 680 Duda, T. F., Morozov, A. K., Howe, B. M., Brown, M. G., Speer, K., Lazarevich,
- 681 P., Worcester, P. F., and Cornuelle, B. D. (2006). “Evaluation of a long-range joint

- 682 acoustic navigation / thermometry system," in *Oceans 2006*, pp. 1–6, <http://files/939/Dudaetal.-2006-EvaluationofaLong-RangeJointAcousticNavigati.pdf> <http://files/940/4099137.html>, doi: [10.1109/OCEANS.2006.306999](https://doi.org/10.1109/OCEANS.2006.306999).
- 685 Duda, T. F., Zhang, W. G., and Lin, Y.-T. (2021). "Effects of Pacific Summer Water layer
686 variations and ice cover on Beaufort Sea underwater sound ducting," *The Journal of the
687 Acoustical Society of America* **149**(4), 2117–2136, doi: [10.1121/10.0003929](https://doi.org/10.1121/10.0003929).
- 688 Duda, T. F., Zhang, W. G., Lin, Y.-T., and Newhall, A. E. (2019). "Long-
689 range sound propagation in the Canada Basin," <http://files/565/Dudaetal.-Unknown-LONG-RANGESOUNDPROPAGATIONINTHECANADABASIN.pdf>.
- 691 Elisseeff, P., Schmidt, H., and Xu, W. (2002). "Ocean acoustic tomography as a data assimilation problem," *IEEE Journal of Oceanic Engineering* **27**(2), 275–282, <http://files/438/Elisseeff,Schmidt,Xu-2002-OceanAcousticTomographyasaDataAssimilationProblem.pdf>, doi: [10.1109/JOE.2002.1002482](https://doi.org/10.1109/JOE.2002.1002482).
- 696 Eustice, R. M., Whitcomb, L. L., Singh, H., and Grand, M. (2006). "Recent advances in
697 synchronous-clock one-way-travel-time acoustic navigation," *Oceans 2006* doi: [10.1109/OCEANS.2006.306931](https://doi.org/10.1109/OCEANS.2006.306931).
- 699 Eustice, R. M., Whitcomb, L. L., Singh, H., and Grund, M. (2007). "Experimental results in synchronous-clock one-way-travel-time acoustic navigation for autonomous underwater vehicles," in *Proceedings - IEEE International Conference on Robotics and Automation*, pp. 4257–4264, <http://files/877/Eusticeetal.-2007-ExperimentalResultsinSynchronous-ClockOne-Way-.pdf> <http://files/877/Eusticeetal.-2007-ExperimentalResultsinSynchronous-ClockOne-Way-.pdf>

- 704 [//files/878/4209752.html](http://files/878/4209752.html), doi: [10.1109/ROBOT.2007.364134](https://doi.org/10.1109/ROBOT.2007.364134).
- 705 Fossum, T. O., Norgren, P., Fer, I., Nilsen, F., Koenig, Z. C., and Ludvigsen, M. (2021).
- 706 “Adaptive sampling of surface fronts in the arctic using an autonomous underwater ve-
- 707 hicle,” IEEE Journal of Oceanic Engineering **46**(4), 1155–1164, doi: [10.1109/JOE.2021.3070912](https://doi.org/10.1109/JOE.2021.3070912).
- 708
- 709 Freitag, L., Ball, K., Partan, J., Koski, P., and Singh, S. (2016). “Long range acoustic
- 710 communications and navigation in the Arctic,” OCEANS 2015 - MTS/IEEE Washington
- 711 2–6, doi: [10.23919/oceans.2015.7401956](https://doi.org/10.23919/oceans.2015.7401956).
- 712 Graupe, C. E., Van Uffelen, L. J., Webster, S. E., Worcester, P. F., and Dzieci-
- 713 uch, M. A. (2019). “Preliminary results for glider localization in the Beau-
- 714 fort Duct using broadband acoustic sources at long range,” in *OCEANS 2019*
- 715 *MTS/IEEE Seattle, OCEANS 2019*, pp. 1–6, <http://files/763/Graupeetal.-2019-Preliminaryresultsforgliderlocalizationinthe.pdf>
- 716 <http://files/763/Graupeetal.-2019-Preliminaryresultsforgliderlocalizationinthe.pdf>
- 717 <http://files/912/>
- 718 <http://files/764/8962637.html> <http://files/913/8962637.html>, doi: [10.23919/OCEANS40490.2019.8962637](https://doi.org/10.23919/OCEANS40490.2019.8962637).
- 719
- 720 Hayes, D. R., and Morison, J. H. (2002). “Determining turbulent vertical velocity, and
- 721 fluxes of heat and salt with an autonomous underwater vehicle,” Journal of Atmospheric
- 722 and Oceanic Technology **19**(5), 759–779.
- 723 Howe, B. M., Miksis-Olds, J., Rehm, E., Sagen, H., Worcester, P. F., and Haral-
- 724 abus, G. (2019). “Observing the Oceans Acoustically,” Frontiers in Marine Science **6**,
- 725 426, <https://www.frontiersin.org/article/10.3389/fmars.2019.00426/full>, doi:

726 10.3389/fmars.2019.00426.

727 Jackson, E. (1983). “Autonomous remotely controlled submersible “ARCS”,” in *Proceedings*
 728 of the 1983 3rd International Symposium on Unmanned Untethered Submersible Technol-
 729 ogy, IEEE, Vol. 3, pp. 77–88.

730 Jakuba, M. V., Roman, C. N., Singh, H., Murphy, C., Kunz, C., Willis, C., Sato,
 731 T., and Sohn, R. A. (2008). “Long-baseline acoustic navigation for under-ice
 732 autonomous underwater vehicle operations,” *Journal of Field Robotics* **25**(11-12),
 733 861–879, <https://onlinelibrary.wiley.com/doi/full/10.1002/rob.20250>
 734 <https://onlinelibrary.wiley.com/doi/abs/10.1002/rob.20250>
 735 <https://onlinelibrary.wiley.com/doi/10.1002/rob.20250>, doi: 10.1002/ROB.20250.

736 Kepper, J. H., Claus, B. C., and Kinsey, J. C. (2017). “MEMS IMU and one-
 737 way-travel-time navigation for autonomous underwater vehicles,” in *OCEANS*
 738 2017 - Aberdeen, Vol. 2017-Octob, pp. 1–9, <http://files/550/Kepper,Claus,Kinsey-2017-MEMSIMUandOne-Way-Travel-TimeNavigationforAutonomousUnderwaterVehicles.pdf>,
 739 doi: 10.1109/OCEANSE.2017.8084842.

741 Krishfield, R., Toole, J., Proshutinsky, A., and Timmermans, M. L. (2008). “Automated
 742 ice-tethered profilers for seawater observations under pack ice in all seasons,” *Journal of*
 743 *Atmospheric and Oceanic Technology* **25**(11), 2091–2105, doi: 10.1175/2008JTECH0587.
 744 1.

745 Kukulya, A., Plueddemann, A., Austin, T., Stokey, R., Purcell, M., Allen, B., Littlefield, R.,
 746 Freitag, L., Koski, P., Gallimore, E. et al. (2010). “Under-ice operations with a remus-100
 747 auv in the arctic,” in *2010 IEEE/OES Autonomous Underwater Vehicles*, IEEE, pp. 1–8.

- 748 Kunz, C., Murphy, C., Camilli, R., Singh, H., Bailey, J., Eustice, R., Jakuba, M., Nakamura,
 749 K., Roman, C., Sato, T., Sohn, R., and Willis, C. (2008). “Deep sea underwater robotic
 750 exploration in the ice-covered Arctic ocean with AUVs,” in *2008 IEEE/RSJ International*
 751 *Conference on Intelligent Robots and Systems*, IEEE, pp. 3654–3660, <http://files/875/Kunzetal.-2008-Deepseaunderwaterroboticexplorationintheice.pdf>
 752 <http://files/968/Kunzetal.-2008-Deepseaunderwaterroboticexplorationintheice.pdf>
 753 <http://ieeexplore.ieee.org/document/4651097/>, doi: [10.1109/IROS.2008.4651097](https://doi.org/10.1109/IROS.2008.4651097).
- 755
- 756 Light, R., and Morison, J. (1989). “The autonomous conductivity-temperture vehicle: First
 757 in the seashuttle family of autonomous underwater vehicle’s for scientific payloads,” in
 758 *Proceedings OCEANS*, Vol. 3, pp. 793–798, doi: [10.1109/OCEANS.1989.586683](https://doi.org/10.1109/OCEANS.1989.586683).
- 759 Litvak, A. (2015). “Acoustics of the deepwater part of the arctic ocean and of russia’s
 760 arctic shelf,” *Herald of the Russian Academy of Sciences* **85**, 239–250, doi: [10.1134/S1019331615030144](https://doi.org/10.1134/S1019331615030144).
- 761
- 762 Mikhalevsky, P. N., Sperry, B. J., Woolfe, K. F., Dzieciuch, M. A., and Worces-
 763 ter, P. F. (2020). “Deep ocean long range underwater navigation,” *The Jour-*
 764 *nal of the Acoustical Society of America* **147**(4), 2365–2382, <http://asa.scitation.org/doi/10.1121/10.0001081>
 765 <http://files/631/Mikhalevskyetal.-2020-Deepeceanlongrangeunderwaternavigation.pdf>, doi: [10.1121/10.0001081](https://doi.org/10.1121/10.0001081).
- 766
- 767 Norgren, P., Lubbad, R., and Skjetne, R. (2014). “Unmanned underwater vehicles in Arctic
 768 operations,” in *22nd IAHR International Symposium on Ice*.

- 769 Paull, L., Saeedi, S., Seto, M., and Li, H. (2014). *AUV navigation and*
 770 *localization: A review*, **39**, pp. 131–149, <http://files/127/Paulletal.-2014-AUVnavigationandlocalizationAreview.pdf>.
- 772 Plueddemann, A. J., Kukulya, A. L., Stokey, R., and Freitag, L. (2012). “Autonomous
 773 Underwater Vehicle Operations Beneath Coastal Sea Ice,” IEEE/ASME Transactions
 774 on Mechatronics **17**(1), 54–64, doi: [10.1109/TMECH.2011.2174798](https://doi.org/10.1109/TMECH.2011.2174798) conference Name:
 775 IEEE/ASME Transactions on Mechatronics.
- 776 Porter, M. B. (2011). “The BELLHOP Manual and User’s Guide,” HLS Research, , 2010
 777 1–57, <http://oalib.hlsresearch.com/Rays/HLS-2010-1.pdf>.
- 778 Poulsen, A. J., and Schmidt, H. (2017). “Acoustic noise properties in the rapidly changing
 779 Arctic Ocean,” **070005**(2016), 070005, doi: [10.1121/2.0000552](https://doi.org/10.1121/2.0000552).
- 780 Randeni, S., Schneider, T., and Schmidt, H. (2020). “Construction of a
 781 high-resolution under-ice AUV navigation framework using a multidisci-
 782 plinary virtual environment,” in *2020 IEEE/OES Autonomous Underwater
 783 Vehicles Symposium, AUV 2020*, pp. 1–7, <http://files/689/Randenietal.-2020-Constructionofahigh-resolutionunder-iceAUVna.pdf>, doi: [10.1109/AUV50043.2020.9267950](https://doi.org/10.1109/AUV50043.2020.9267950).
- 786 Randeni, S., Schneider, T., Schmidt, H., Bhatt, E., and Viquez, O. (2021). “A high-
 787 resolution AUV navigation framework with integrated communication and tracking for
 788 under-ice deployments,” *Field Robotics* (in review).
- 789 Rossby, T., Dorson, D., and Fontaine, J. (1986). “The RAFOS System,” *Journal of Atmo-*
 790 *spheric and Oceanic Technology* **3**, 148–162.

- 791 Rypkema, N. R., Fischell, E. M., and Schmidt, H. (2017). “One-Way Travel-Time Inverted
 792 Ultra-Short Baseline Localization for Low-Cost Autonomous Underwater Vehicles,” in *2017*
 793 *IEEE International Conference on Robotics and Automation (ICRA)*, Singapore, pp. 4920–
 794 4926.
- 795 Schmidt, H., and Schneider, T. (2016). “Acoustic communication and navigation in
 796 the new Arctic-A model case for environmental adaptation,” 3rd Underwater Com-
 797 munications and Networking Conference, Ucomms 2016 <http://files/583/Schmidt,Schneider-2016-AcousticCommunicationandNavigationintheNewArctic-AModelCaseforEnvironment.pdf>, doi: [10.1109/UComms.2016.7583469](https://doi.org/10.1109/UComms.2016.7583469).
- 800 Schneider, T., and Schmidt, H. (2018). “NETSIM: A realtime virtual ocean hardware-
 801 in-the-loop acoustic modem network simulator,” in *2018 4th Underwater Communi-*
 802 *cations and Networking Conference, UComms 2018*, pp. 1–5, <http://files/1047/SchneiderandSchmidt-2018-NETSIMARealtimeVirtualOceanHardware-in-the-l.pdf>, doi: [10.1109/UComms.2018.8493188](https://doi.org/10.1109/UComms.2018.8493188).
- 805 Schneider, T., Schmidt, H., and Randeni, S. (2020). “Self-Adapting Under-Ice Inte-
 806 grated Communications and Navigation Network,” 2020 5th Underwater Communica-
 807 tions and Networking Conference, UComms 2020 5, <http://files/607/Schneideretal.-Self-AdaptingUnder-IceIntegratedCommunications.pdf>.
- 809 Singh, S., Grand, M., Bingham, B., Eustice, R., Singh, H., and Freitag, L. (2006).
 810 “Underwater acoustic navigation with the WHOI Micro-Modem,” in *Oceans 2006*,
 811 IEEE, pp. 1–4, <http://ieeexplore.ieee.org/document/4099008/>, doi: [10.1109/OCEANS.2006.1700001](https://doi.org/10.1109/OCEANS.2006.1700001).
 812 [Singhetal.-2006-UnderwaterAcousticNavigationwiththeWHOIMicro.pdf](http://files/774/Singhetal.-2006-UnderwaterAcousticNavigationwiththeWHOIMicro.pdf), doi: [10.1109/OCEANS.2006.1700001](https://doi.org/10.1109/OCEANS.2006.1700001).

813 1109/OCEANS.2006.306853.

814 Timmermans, M.-L., and Winsor, P. (2013). “Scales of horizontal density structure in the
 815 chukchi sea surface layer,” Continental Shelf Research **52**, 39–45.

816 Toole, J. M., Krishfield, R. A., Timmermans, M. L., and Proshutinsky, A. (2011). “The
 817 Ice-Tethered profiler: Argo of the Arctic,” Oceanography **24**(3), 126–135, doi: [10.5670/oceanog.2011.64](https://doi.org/10.5670/oceanog.2011.64).

819 Uffelen, L. J. V., Howe, B. M., Nosal, E.-M., Carter, G. S., Worcester, P. F., and Dzieciuch,
 820 M. A. (2016). “Localization and subsurface position error estimation of gliders using
 821 broadband acoustic signals at long range,” IEEE Journal of Oceanic Engineering **41**(3),
 822 501–508.

823 Van Uffelen, L. J. (2021). “Global Positioning Systems: Over Land and Under Sea,” Acoustics
 824 Today **17**(1), 52, doi: [10.1121/at.2021.17.1.52](https://doi.org/10.1121/at.2021.17.1.52).

825 Van Uffelen, L. J., Nosal, E.-M., Howe, B. M., Carter, G. S., Worcester, P. F., Dzieciuch,
 826 M. A., Heaney, K. D., Campbell, R. L., and Cross, P. S. (2013). “Estimating uncertainty
 827 in subsurface glider position using transmissions from fixed acoustic tomography sources,”
 828 The Journal of the Acoustical Society of America **134**(4), 3260–3271, doi: [10.1121/1.4818841](https://doi.org/10.1121/1.4818841).

830 Webster, S. E., Eustice, R. M., Singh, H., and Whitcomb, L. L. (2009). “Preliminary
 831 deep water results in single-beacon one-way-travel-time acoustic navigation
 832 for underwater vehicles,” 2009 IEEE/RSJ International Conference on Intelligent
 833 Robots and Systems, IROS 2009 2053–2060, <http://files/416/Websteretal.-2009-Preliminarydeepwaterresultsinsingle-beaconone-way-travel-timeacousticnavigationf>

- 835 pdf, doi: [10.1109/IROS.2009.5354457](https://doi.org/10.1109/IROS.2009.5354457).
- 836 Webster, S. E., Eustice, R. M., Singh, H., and Whitcomb, L. L. (2012). “Advances in
 837 single-beacon one-way-travel-time acoustic navigation for underwater vehicles,” Interna-
 838 tional Journal of Robotics Research **31**(8), 935–950, doi: [10.1177/0278364912446166](https://doi.org/10.1177/0278364912446166).
- 839 Webster, S. E., Freitag, L. E., Lee, C. M., and Gobat, J. I. (2015). “Towards real-time
 840 under-ice acoustic navigation at mesoscale ranges,” in *Proceedings - IEEE International
 841 Conference on Robotics and Automation*, June, IEEE, pp. 537–544, [http://files/625/
 842 Websteretal.-2015-Towardsreal-timeunder-iceacousticnavigationat.pdf](http://files/625/Websteretal.-2015-Towardsreal-timeunder-iceacousticnavigationat.pdf)
 843 <http://files/641/Websteretal.-2015-Towardsreal-timeunder-iceacousticnavigationat.pdf>
- 844 <http://files/835/Websteretal.-2015-Towardsreal-timeunde>, doi: [10.1109/ICRA.2015.7139231](https://doi.org/10.1109/ICRA.2015.7139231).
- 845 Wu, M., Barmin, M. P., Andrew, R. K., Weichman, P. B., White, A. W., Lavely, E. M.,
 846 Dzieciuch, M. A., Mercer, J. A., Worcester, P. F., and Ritzwoller, M. H. (2019).
 847 “Deep water acoustic range estimation based on an ocean general circulation model:
 848 Application to PhilSea10 data,” The Journal of the Acoustical Society of America
 849 **146**(6), 4754–4773, [https://asa.scitation.org/doi/10.1121/1.5138606](https://doi.org/10.1121/1.5138606)
 850 <http://files/947/Wuetal.-2019-Deepwateracousticrangeestimationbasedonano.pdf>
 851 <http://files/948/1.html>, doi: [10.1121/1.5138606](https://doi.org/10.1121/1.5138606).